**Proceedings of the ASME 2011 International Mechanical Engineering Congress & Exposition**
**IMECE2011**
**November 11-17, 2011, Denver, Colorado, USA**

**IMECE2011-62049**

# Simulation of 3D Multistage Axial Compressor Using a Fully Conservative Sliding Boundary Condition

**Hongsik IM** [*], **Xiangying Chen** [†], **Gecheng Zha** [‡]
Dept. of Mechanical and Aerospace Engineering
University of Miami
Coral Gables, Florida 33124
E-mail: gzha@miami.edu

*Multistage 3D steady and unsteady viscous computations are conducted for a transonic axial compressor with an IGV, rotor and stator blade row. A fully conservative sliding technique is developed with high order shock capturing schemes to better capture the interaction between stationary and rotating blade row. A 1/7th annulus is used for the unsteady simulation with a phase lag BC. For comparison purpose, a steady simulation of the same multistage compressor with single blade passage is performed using the mixing plane approach. It is shown that the sliding BC captures wake propagation very well in the interaction between blade rows. The unsteady multistage simulation using sliding BC and phase lag BC predicts almost identical loading distribution to the steady state simulation at the mid-span, but have significant loading distribution difference at tip section.*

## 1 Introduction

The interaction between rotating and stationary blades introduces inherent unsteadiness to the flow of multistage turbomachinery. There are typically two approaches to treat two adjacent blade rows in relative rotation frame; mixing plane and sliding interface.

Mixing plane method has been widely used due to its simplicity. Denton [1], Dawes [2], Singh [3], and Chen [4] used mixing plane approach to calculate multistage machines. In this approach the circumferential-averaging is typically used in order to achieve the radial profiles and conserve the mass flow. Most researchers [1–4] exchange the flow data between two blade rows using less than two cells for the mixing BC. Gerolymos et al. [5] overlapped multiple phantom cells where the averaged quantities of the opposite domain are stored. There are two major disadvantages that arise with mixing plane. First, mixing plane generates artificial mixing loss [6] due to averaging the non-uniform flow at the mixed-out and mixed-in plane. Second, the effects of unsteady interaction between inter-blade rows could not be taken into account. Barter et al. [4] presented an effect of unsteady interaction that changes the blade loading of the upstream blade in a multistage transonic turbine.

Sliding interface methods are often used for multi-stage unsteady rotor-stator interaction. For instance, the shock wave interaction between the inter blade rows as well as rotating instabilities such as NSV(Non-Synchronous Vibration) and rotating stall can be predicted not by the steady approach, but only by the conservative unsteady approach. Numerous studies on the unsteady rotor/stator interaction has been developed [7–10] based on interpolation on the rotor-stator interface. Rai [7] used the patched and overlaid grid system based on interpolation to solve an axial turbine with a rotor-stator configuration. Chen et al. [11] pointed out that lack of flux conservation can significantly affect the solution accuracy where shock interaction exists between the blade rows. The fact is the methods of rotor/stator interaction using any type of interpolation methods can not satisfy the conservation of the flux across the interface.

The phase-lagged technique for periodic circumferential boundaries can dramatically reduce computational efforts since it enables the use of the reduced model instead of full annulus simulation. The phase-lagged methods are based on the assumption that if two adjacent blades oscillate with a phase difference, the fluid flow at the boundaries associated with these blades will also vary in time with the same phase. The conventional way to treat the phase shifted boundary is a direct store method suggested by Erods et al. [12]. In this method the flow variables on the periodic surface are stored over the oscillation. These data are then used to update the corresponding periodic boundary with a time lag. This method is simple, but requires large computer memory.

In this study three major simulation techniques for the multistage turbomachinery are developed and implemented;

[*] Graduate Student, AIAA Member
[†] Research Associate Professor, AIAA Member
[‡] Associate Professor, ASME Senior Member

a mixing plane, a sliding BC, and the phase lag BC suggested by He [13]. The multistage axial compressor designed by General Electric is used for the steady/unsteady simulations. The steady simulation for a single passage of IGV, rotor, and stator is performed using the mixing plane. Using the sliding BC, the unsteady simulation is carried out for the 1/7th annulus that satisfies the geometric periodicity.

For transonic multi-blade row numerical simulation, low diffusion and shock capturing capability have large impacts on the accuracy due to the shock wave interaction with boundary layer and tip vortices and, wake propagation. For example, Gerolymos et al. [5] applied the MUSCL Van Leer flux vector splitting with Van Albada limiters to solve a four stage axial turbine at a off-design point where strong coupling of the flow field between the blade rows is dominant. Comparison of CFD and experiment shows that the mixing plane overestimated efficiency by about 2%, and the predicted radial profiles such as total pressure, total temperature, and flow angle shows large discrepancy compared to the experiment.

In the present study, the Low Diffusion E-CUSP (LDE) Scheme [14] as an accurate shock capturing Riemann solver is used to resolve the unsteady interaction between the blade rows. The LDE scheme can capture crisp shock profile and exact contact surface discontinuities as accurately as the Roe scheme [15]. However, it is simpler and more CPU efficient than the Roe scheme due to no matrix operation. The 3rd order WENO reconstruction for the inviscid flux and 2nd order central differencing for the viscous terms [16] are used. An implicit unfactored Gauss-Seidel line iteration is used to achieve high convergence rate. The high-scalability parallel computing is applied to save wall clock time [17].

**Nomenclature**

| | |
|---|---|
| $a$ | speed of sound, $\sqrt{\gamma p/\rho}$ |
| $C_m$ | meridional absolute velocity, $\sqrt{C_x^2+C_r^2}$ |
| $C_x, C_\theta, C_r$ | absolute velocities in $x$, $\theta$, $r$ direction |
| $d$ | distance from the closest wall |
| $\mathbf{E}, \mathbf{F}, \mathbf{G}$ | inviscid flux vectors in $\xi, \eta, \zeta$ direction |
| $\mathbf{E}_v, \mathbf{F}_v, \mathbf{G}_v$ | viscous flux vectors in $\xi, \eta, \zeta$ direction |
| $e$ | total energy per unit mass |
| $J$ | Jacobian of the coordinate transformation |
| $I$ | Identity matrix |
| $L_\infty$ | blade chord at hub |
| $\mathbf{l}$ | normal vector on $\xi$ surface with its magnitude equal to the elemental surface area and pointing to the direction of increasing $\xi$ |
| $l_t$ | grid moving velocity |
| $M_\infty$ | reference Mach number, $\frac{U_\infty}{a_\infty}$ |
| $p_o$ | total pressure |
| $Pr$ | Prandtl number |
| $Pr_r$ | turbulent Prandtl number |
| $\mathbf{Q}$ | conservative variable vector |
| $q_k$ | total heat flux in Cartesian coordinates |
| $R_e$ | Reynolds number, $\frac{\rho_\infty U_\infty L_\infty}{\mu_\infty}$ |
| $R_o$ | Rossby number, $\frac{\Omega L_\infty}{U_\infty}$ |
| $T_o$ | total temperature |
| $U, V, W$ | contravariant velocities in $\xi, \eta, \zeta$ direction |
| $U_\infty$ | reference velocity |
| $\mathbf{V}$ | relative velocity vector |
| $V_x, V_\theta, V_r$ | relative velocities in $x$, $\theta$, $r$ direction |
| $y^+$ | dimensionless wall normal distance |
| $\alpha$ | swirl angle, $tan^{-1}(C_\theta/C_m)$ |
| $\beta$ | pitch angle, $tan^{-1}(C_r/C_x)$ |
| $\Delta t$ | physical time step |
| $\delta_{ik}$ | Kronecker delta function |
| $\mu_t$ | turbulent eddy viscosity |
| $\nu$ | kinematic viscosity |
| $\tilde{\nu}$ | working variable of the S-A model related to turbulent eddy viscosity |
| $\Omega$ | rotor angular frequency in *radians/sec* |
| $\tau_{ik}$ | shear stress in Cartesian coordinates |

**Subscripts**

| | |
|---|---|
| $i, j, k$ | indices |
| $o$ | stagnation conditions |
| $\infty$ | reference variable at rotor inlet |

**Abbreviation**

| | |
|---|---|
| *IGV* | inlet guide vane |
| *BC* | boundary condition |

## 2 Navier-Stokes Equations in a Rotating Frame

The governing equations solved in this study are the equation of motion of fluid flow for turbomachinery in a relative frame of reference, which can be derived by adding the effects of coriolis force $(2\Omega\times\mathbf{V})$ and the centrifugal force$(\Omega\times\Omega\times\mathbf{r})$ to the equation for the absolute frame. Expanding this momentum equation with continuity and energy equations in a rotating Cartesian system$(x,y,z)$ as shown in Fig. 1 and applying coordinate transformation to the generalized coordinate system$(\xi,\eta,\zeta)$, the dimensionless Reynolds-averaged 3D Navier-Stokes equations with the SA(Spalart-Allmaras) turbulence model [18] can be expressed as the following conservative form:

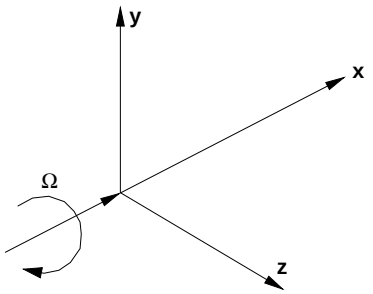


Fig. 1: The Cartesian system with y and z axes rotation about the x-axis at a constant speed $\Omega$

$$\frac{\partial \mathbf{Q}}{\partial t}+\frac{\partial \mathbf{E}}{\partial \xi}+\frac{\partial \mathbf{F}}{\partial \eta}+\frac{\partial \mathbf{G}}{\partial \zeta}=\frac{1}{R_e}\left(\frac{\partial \mathbf{E_v}}{\partial \xi}+\frac{\partial \mathbf{F_v}}{\partial \eta}+\frac{\partial \mathbf{G_v}}{\partial \zeta}+\mathbf{S}\right) \quad (1)$$

The conservative variable vector $\mathbf{Q}$, inviscid flux vector $\mathbf{E}$, the viscous flux vector $\mathbf{E_v}$ and the source term vector $\mathbf{S}$ are expressed as follows and the rest can be expressed following the symmetric rule.

$$\mathbf{Q}=\frac{1}{J}\begin{pmatrix}\bar{\rho}\\ \bar{\rho}\tilde{u}\\ \bar{\rho}\tilde{v}\\ \bar{\rho}\tilde{w}\\ \bar{\rho}\tilde{e}\\ \bar{\rho}\tilde{\nu}\end{pmatrix} \quad (2)$$

$$\mathbf{E}=\begin{pmatrix}\bar{\rho}U\\ \bar{\rho}\tilde{u}U+l_x\bar{p}\\ \bar{\rho}\tilde{v}U+l_y\bar{p}\\ \bar{\rho}\tilde{w}U+l_z\bar{p}\\ (\bar{\rho}\tilde{e}+\bar{p})U-l_t\bar{p}\\ \bar{\rho}\tilde{\nu}U\end{pmatrix} \quad (3)$$

$$\mathbf{E_v}=\begin{pmatrix}0\\ l_k\bar{\tau}_{xk}\\ l_k\bar{\tau}_{yk}\\ l_k\bar{\tau}_{zk}\\ l_k(\tilde{u}_i\bar{\tau}_{ki}-\bar{q}_k)\\ \frac{\bar{\rho}}{\sigma}(\nu+\tilde{\nu})(\mathbf{l}\bullet\nabla\tilde{\nu})\end{pmatrix} \quad (4)$$

$$\mathbf{S}=\frac{1}{J}\begin{pmatrix}0\\ 0\\ \bar{\rho}R_eR_o{}^2y+2\bar{\rho}R_eR_ow\\ \bar{\rho}R_eR_o{}^2z-2\bar{\rho}R_eR_ov\\ 0\\ \bar{\rho}C_{b1}(1-f_{t2})\tilde{S}\tilde{\nu}+\\ \frac{1}{Re}\left[-\bar{\rho}\left(C_{w1}f_w-\frac{C_{b1}}{\kappa^2}f_{t2}\right)\left(\frac{\tilde{\nu}}{d}\right)^2\right.\\ \left.+\frac{\bar{\rho}}{\sigma}C_{b2}(\nabla\tilde{\nu})^2-\frac{1}{\sigma}(\nu+\tilde{\nu})\nabla\tilde{\nu}\bullet\nabla\bar{\rho}\right]\\ +Re\left[\bar{\rho}f_{t1}(\Delta q)^2\right]\end{pmatrix} \quad (5)$$

where the overbar denotes the Reynolds-averaged quantity, and the tilde is used to denote the Favre averaged quantity. $U$, $V$ and $W$ are the contravariant velocities in $\xi$, $\eta$, $\zeta$ directions. For example, $U$ is defined as follows.

$$U=l_t+\mathbf{l}\bullet\mathbf{V}=l_t+l_x\tilde{u}+l_y\tilde{v}+l_z\tilde{w} \quad (6)$$

where

$$l_t=\frac{\xi_t}{J}d\eta d\zeta, \qquad l=\frac{\nabla\xi}{J}d\eta d\zeta \quad (7)$$

When the grid is stationary, $l_t=0$. In the current discretization, $\Delta\xi=\Delta\eta=\Delta\zeta=1$.

The shear stress $\bar{\tau}_{ik}$ and total heat flux $\bar{q}_k$ in Cartesian coordinates is given by

$$\bar{\tau}_{ik}=(\mu+\mu_t)\left[\left(\frac{\partial\tilde{u}_i}{\partial x_k}+\frac{\partial\tilde{u}_k}{\partial x_i}\right)-\frac{2}{3}\delta_{ik}\frac{\partial\tilde{u}_j}{\partial x_j}\right] \quad (8)$$

$$\bar{q}_k=-\left(\frac{\mu}{Pr}+\frac{\mu_t}{Pr_t}\right)\frac{\partial\tilde{T}}{\partial x_k} \quad (9)$$

where $\mu$ is determined by Sutherland's law. The above equations are in the tensor form, where the subscripts $i,k$ represents the coordinates $x,y,z$ and the Einstein summation convention is used. Eq.(8) and (9) are transformed to the generalized coordinate system. The turbulent eddy viscosity $\mu_t$ is determined by the SA one equation turbulence model as the following:

$$\mu_t=\bar{\rho}\tilde{\nu}f_{v1} \quad (10)$$

where

$$f_{v1}=\frac{\chi^3}{\chi^3+c_{v1}^3}, \quad \chi=\frac{\tilde{\nu}}{\nu}$$
$$r=\frac{\tilde{\nu}}{R_e\tilde{S}k^2d^2}, \quad \tilde{S}=S+\frac{\tilde{\nu}}{R_ek^2d^2}f_{v2}, \quad f_{v2}=1-\frac{\chi}{1+\chi f_{v1}}$$
$$S=\sqrt{2\omega_{ij}\omega_{ij}}, \quad \omega_{ij}=\frac{1}{2}\left(\frac{\partial u_i}{\partial x_j}-\frac{\partial u_j}{\partial x_i}\right)$$

The rest of auxiliary relations and the values of the coefficients given by reference [19] are used.

The normalized equation of state as a constitutive equation relating density to pressure and temperature in the relative frame is defined as

$$\bar{\rho}\tilde{e}=\frac{\bar{p}}{(\gamma-1)}+\frac{1}{2}\bar{\rho}(\tilde{u}^2+\tilde{v}^2+\tilde{w}^2)-\frac{1}{2}\bar{\rho}r^2R_o{}^2 \quad (11)$$

where $r$ $(=\sqrt{y^2+z^2})$ is the normalized radius from the rotating axis, $x$ in this study. For simplicity, all the bar and tilde

in above equations will be dropped in the rest of this paper.

### 2.1 Implicit Time Marching Scheme

The 2nd order implicit method is used with the dual time stepping method [16, 20]. A pseudo temporal term $\frac{\partial Q}{\partial \tau}$ is added to the governing equation Eq. (1). This term vanishes at the end of each physical time step and has no influence on the accuracy of the solution. The pseudo temporal term is discretized with first order Euler scheme. Let $m$ stand for the iteration index within a physical time step, the semi-discretized governing equation can be expressed as

$$\left[\left(\frac{1}{\Delta\tau}+\frac{1.5}{\Delta t}\right)I-\left(\frac{\partial R}{\partial \mathbf{Q}}\right)^{n+1,m}\right]\delta\mathbf{Q}^{\mathbf{n+1,m+1}} = R^{n+1,m}-\frac{3\mathbf{Q}^{\mathbf{n+1,m}}-4\mathbf{Q}^{\mathbf{n}}+\mathbf{Q}^{\mathbf{n-1}}}{2\Delta t} \tag{12}$$

where $\Delta\tau$ is the pseudo time step, and R is the net flux of the discretized Navier-Stokes equations.

## 3 Mixing Plane for Steady Rotor/Stator Interface

A mixing plane technique is implemented using the ghost cell approach as sketched in Fig. 2. The conservative variables are averaged and stored to the corresponding ghost cells of the adjacent domain using the following relations between the moving frame and the fixed frame. For example, the flow quantities of the cell $n-1$, and $n$ in the fixed domain are volume averaged circumferentially, and then stored to the ghost cell $m+2$, and $m+1$ in the moving domain. This method couples two domains and facilitates higher order spatial schemes at the interface.

$$\begin{pmatrix}\bar{\rho}\\ \bar{\rho}\bar{U}\\ \bar{\rho}\bar{V}_r\\ \bar{\rho}(\bar{W}_\theta+rR_o)\\ \bar{\rho}\bar{e}+\bar{\rho}\bar{V}_\theta rR_o\\ \bar{\rho}\bar{\tilde{\nu}}\end{pmatrix}_{Fixed} = \begin{pmatrix}\bar{\rho}\\ \bar{\rho}\bar{U}\\ \bar{\rho}\bar{V}_r\\ \bar{\rho}\bar{W}_\theta\\ \bar{\rho}\bar{e}\\ \bar{\rho}\bar{\tilde{\nu}}\end{pmatrix}_{Moving} \tag{13}$$

where the overbar denotes volume-averaged variables as

$$\bar{\Phi}=\frac{1}{V}\int\int\int_{SR}\Phi dV \tag{14}$$

As aforementioned, the circumferential average cut off the wake propagation and add artificial mixing loss to the calculation. However, the mixing plane method is convenient to couple multi-stage computation.

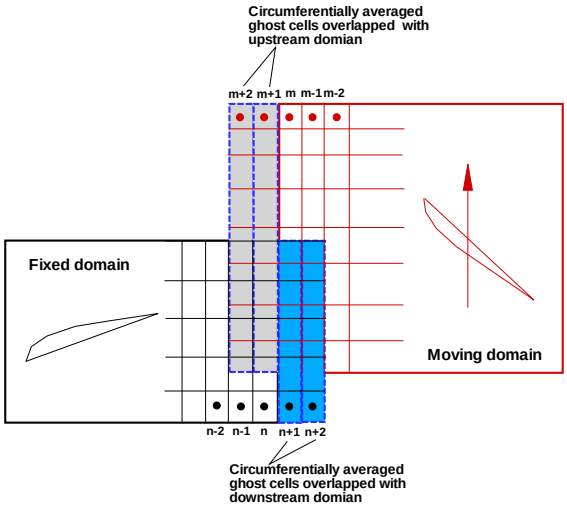


Fig. 2: Ghost cell approach for mixing plane

## 4 Sliding Interface for Unsteady Rotor/Stator Interaction

An accurate high order scheme in space is necessary for multistage axial compressors in order to rigorously resolve interaction effects such as wake and shocks between rotor (rotating blade) and stator (stationary blade). A conservative sliding BC without interpolation is developed to solve the moving rotor in the rotating frame and the stationary blades in the fixed frame. The relations between the moving frame and the fixed frame are used for the information exchange.

$$\begin{pmatrix}\rho\\ \rho U\\ \rho V_r\\ \rho(W_\theta+rR_o)\\ \rho e+\rho V_\theta rR_o\\ \rho\tilde{\nu}\end{pmatrix}_{Fixed} = \begin{pmatrix}\rho\\ \rho U\\ \rho V_r\\ \rho W_\theta\\ \rho e\\ \rho\tilde{\nu}\end{pmatrix}_{Moving} \tag{15}$$

The conservative variables $\rho, \rho U, \rho V_r, \rho V_\theta$, $\rho e$, and $\rho\tilde{\nu}$ are exchanged dynamically when the moving domains slide and are updated in every physical time step. Since the sliding BC with the ghost cell approach can ensure the boundary cells to be solved in the same manner as the inner domain, it hence can capture the interactive effects between the rotor and the stator.

The condition for this sliding BC to avoid interpolation across the sliding BC is to use a one-to-one matched grid at the interface. Two domains at the interface have to have the same mesh size and also the grid points should be evenly distributed circumferentially. This condition can be always satisfied if it is fully annulus calculation. If it is for a sector of the annulus, a geometrically periodic sector should be used first if available. In this case, the grid size of the interface disk in the rotor circumferential direction can be found by the greatest common factor(GCF). For example, if we have a compressor with the number of IGV 56 and the number

of rotor 35, on can reduce the full annulus to 1/7th annulus with 8 IGV blades and 5 rotor blades that satisfies the geometry periodicity. Then, the GCF is 40 as 5 multiples per IGV blade and 8 multiples per rotor blade can meet the matching condition for both domains. In case a geometric periodicity for a sector of the full annulus does not exist, a sector being closest to a geometric periodicity may be used based on the best judgement. When the rotating blades are moving, the mesh of the moving blades are moving with the blades. The one-to-one connection of the two grid points from the stationary blade to the moving blade at the sliding interface will remain on the same grid points when the circumferential distance is small. When the circumferential distance of the two grid points is greater than half of the interval due to the moving blades, the connection will switch to the next grid point so that all the grid points remain one-to-one connected without much mesh skewness. This process will keep being repeated in the rotor-stator sliding interface during the calculation.

Fig. 3 illustrates algorithm of the sliding BC. Let the rotor domain be rotated by two cells from the initial position. Then, the cell 1 to 4 on the rotor side and the cell 3 to 6 on the stator side are matched and exchanged, while the cell 5 and 6 of the rotor domain and the cell 1 and 2 of the stator domain have no cells to exchange. Therefore, we define the exchange array of those cells using a periodic rotation rule. For instance, the rotor cell 5 and 6 are rotated by the angle($\phi$) and are exchanged with the stator cell 1 and 2.

The rotating mesh may not be matched with the stator domain like staggered grid at the interface. Mostly the interpolation is necessary to find out the exact point for the information exchange. However, it needs more computational cost and storage. We employ the conservative cell exchange technique to reduce the computational efforts and to fully conserve data exchange. The rotated mesh is located to the closest cell of the counterpart domain. When $\Delta t$ is larger than one circumferential grid cell spacing that has domain pass a few cells, likely more pseudo time steps are needed.

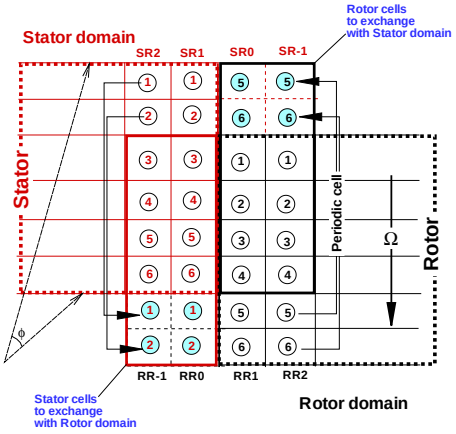


Fig. 3: Rotor/Stator interface exchange algorithm

## 5 Circumferential Fourier Phase-lagged BC

An efficient circumferential phase-lagged boundary condition is implemented for the multi-blade passage or single blade passage simulations. He and Denton [13] proposed a shape-correction method where the variation in fluid properties over an oscillation cycle is decomposed into its Fourier coefficients. This method needs much less computer storage compared to the direct store method [12] because only the coefficients are stored to update the variables.

Since the present solver uses the ghost cell approach at boundaries as sketched in Fig.4, the Cell $GL$(ghost cell of the lower periodic boundary) corresponds to the cell $IU$(inner cell of the upper periodic boundary), and vice versa for the cell $GU$ and the cell $IL$. One can write a $N_{th}$ order timewise Fourier series for the conservative variable vector($Q$) if the rotor rotates from the lower to the upper boundary with the phase angle($\phi$) as

$$Q_{GL(x,t)} = \bar{Q}_{IU(x)} + \sum_{n=1}^{N} [An_{IU} \cdot sin[n(\omega t + \phi)] + Bn_{IU} \cdot cos[n(\omega t + \phi)]] \quad (16)$$

$$Q_{GU(x,t)} = \bar{Q}_{IL(x)} + \sum_{n=1}^{N} [An_{IL} \cdot sin[n(\omega t - \phi)] + Bn_{IL} \cdot cos[n(\omega t - \phi)]] \quad (17)$$

where

$$An_{IL} = \frac{\omega}{2\pi} \sum_{j=1}^{NP} Q(t)_{IL} \cdot sin(n\omega t)\Delta t \quad (18)$$

$$An_{IU} = \frac{\omega}{2\pi} \sum_{j=1}^{NP} Q(t)_{IU} \cdot sin(n\omega t)\Delta t \quad (19)$$

$$Bn_{IL} = \frac{\omega}{2\pi} \sum_{j=1}^{NP} Q(t)_{IL} \cdot cos(n\omega t)\Delta t \quad (20)$$

$$Bn_{IU} = \frac{\omega}{2\pi} \sum_{j=1}^{NP} Q(t)_{IU} \cdot cos(n\omega t)\Delta t \quad (21)$$

where the overbar denotes a time-averaged variables, $\omega(= 2\pi/T)$ is the blade vibration frequency(or blade passing frequency), $n$ is the harmonic number, and $NP(= T/\Delta t)$ is the number of steps taken over one oscillation cycle.

The Fourier coefficients are calculated over one time period using an approximate integral technique, the trapezoidal rule. This means these coefficients are lagged by one cy-

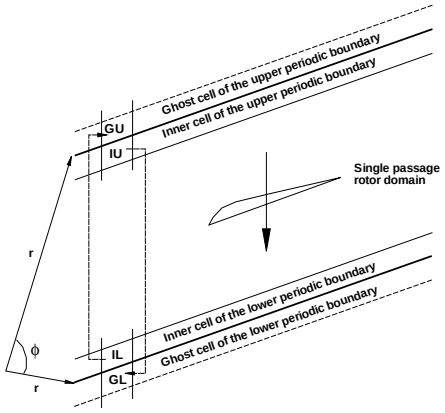


Fig. 4: Sketch of Fourier phase lag domain

cle and no coefficient is available for the first cycle. For the first vibration cycle the upper and lower boundaries are considered periodic, and hence one can update the Fourier coefficients over every time period from the second period. Notice that this phase lag BC implemented includes inherently the nonlinear interactions between the time-averaged flow and the unsteady disturbances [21]. Current phase lag BC has been validated using a full annulus flutter simulation for NASA rotor 67 [22].

## 6 Other Boundary Conditions

It is convenient for turbomachinery to express the boundary conditions in Cylindrical system. Coordinates mapping between the Cartesian $(x,y,z)$ and Cylindrical system$(x,\theta,r)$ is given as

$$\begin{pmatrix} V_x \\ V_\theta \\ V_r \end{pmatrix} = \begin{pmatrix} u \\ v\cdot sin\theta - w\cdot cos\theta \\ v\cdot cos\theta + w\cdot sin\theta \end{pmatrix} = \begin{pmatrix} u \\ \frac{v\cdot z - w\cdot y}{r} \\ \frac{v\cdot y + w\cdot z}{r} \end{pmatrix} \tag{22}$$

where $u$, $v$, and $w$ are the relative velocity components in the $x$, $y$, and $z$ coordinate directions respectively. The absolute velocity components$(C_x,C_\theta,C_r)$ are related to the relative velocity components$(V_x,V_\theta,V_r)$ using the rotor wheel speed$(r\Omega)$ as

$$\begin{pmatrix} C_x \\ C_\theta \\ C_r \end{pmatrix} = \begin{pmatrix} V_x \\ V_\theta - rR_o \\ V_r \end{pmatrix} \tag{23}$$

At the IGV inlet, the radial distributions of total pressure $P_o$, total temperature $T_o$, swirl angle $\alpha$ and pitch angle $\beta$ are specified. The velocity is taken from the computational domain by the extrapolation in order to determine the rest of variables. First, we assume that the speed of sound $a$ is constant at the inlet boundary. Then, the static temperature is obtained by

$$T_b = T_o[1 - \frac{\gamma-1}{2}(\frac{C_i}{a_o})^2] \tag{24}$$

where the subscripts $i$ represents the first interior cell and subscripts $b$ indicates the first ghost cell of the boundary. $C_i$ is the absolute velocity of the first interior cell and $a_o$ is the total speed of sound defined by

$$\frac{a_o^2}{\gamma-1} = \frac{a_i^2}{\gamma-1} + \frac{C_i^2}{2} \tag{25}$$

Using the isentropic relations, the absolute velocity$(C_b)$, the static pressure$(p_b)$ and density$(\rho_b)$ are determined by

$$|C_b| = \frac{1}{M_\infty}\sqrt{\frac{2}{\gamma-1}(T_o - T_b)} \tag{26}$$

$$p_b = P_o\left(\frac{T_b}{T_o}\right)^{\frac{\gamma}{\gamma-1}} \tag{27}$$

$$\rho_b = \frac{p_b\gamma}{a_b^2} \tag{28}$$

Then, the velocity components are decoupled and the conservative variables are found as the following:

$$\begin{pmatrix} \rho \\ \rho V_x \\ \rho V_r \\ \rho V_\theta \\ \rho e \end{pmatrix}_b = \begin{pmatrix} \rho_b \\ \rho_b C_m\cdot cos\beta \\ \rho_b C_m\cdot sin\beta \\ \rho_b(C_m\cdot tan\alpha - rR_o) \\ \frac{p_b}{(\gamma-1)} + \frac{\rho_b}{2}(V_x^2 + V_r^2 + V_\theta^2 - r^2R_o^2) \end{pmatrix} \tag{29}$$

At the stator outlet, the static pressure$(p_b)$ is specified in the spanwise direction. The components of velocity$(u,v,w)$ are extrapolated from the computational domain. Then, to update the density$(\rho_b)$ by using the following isentropic relation.

$$\rho_b = \left(\frac{p_b}{p_i}\right)^{\frac{1}{\gamma}}\rho_i \tag{30}$$

where $p_i$ is the static pressure and $\rho_i$ is the density at the first interior cell of the outlet boundary. The total energy is updated based on $p_b$ and $\rho_b$.

On the solid wall, the non-slip boundary condition is applied to enforce mass flux going through the wall to be zero. The velocity components of the ghost cells are obtained by the extrapolation between the moving wall velocity and interior cells as follows:

$$\vec{V}_b = 2\vec{V}_w - \vec{V}_i \tag{31}$$

where $\vec{V}_b$ denotes the ghost cell velocity, $\vec{V}_i$ stands for the velocity of $1st$ interior cell close to the wall, and $\vec{V}_w$ is wall moving velocity given by $\vec{\Omega} \times \vec{r}$. Another option to save mesh size in our computation is to use the law of the wall. When $y^+$ is between 11 and 300, the no slip condition is replaced by using the wall function.

$$u^+ = \frac{1}{k} ln y^+ + B \tag{32}$$

where $k$ denotes Von K*á*rm*á*n constant taken as 0.41, and $B$ denotes a dimensionless constant corresponding to the wall roughness taken as 5.0. If the wall surface is $\eta$ direction, the wall static pressure for the inviscid momentum equation can be determined by the following manner.

$$\frac{\partial p}{\partial \eta} = \frac{\rho_i}{\sqrt{\eta_x^2+\eta_y^2+\eta_z^2}} \frac{V_\theta^2}{r} \tag{33}$$

If the wall surface is stationary, then the static pressure gradient across the wall boundary is set to zero. In addition, the adiabatic condition($\partial T/\partial \eta = 0$) is used to impose zero heat flux through the wall.

## 7 Steady Simulation

Using the mixing plane, the single passage steady computations are performed with CFL number of 1. In-phase condition was applied at periodic boundary. The computational mesh is presented in Fig. 5. The rotor tip clearance of about 2.4% tip chord was given. The rotor tip is precisely modeled with 21 grid points using a O-mesh block. The mesh of IGV/rotor/stator is partitioned to total 30 blocks for parallel computation. The mesh around blade was constructed by using the O-mesh. The H-mesh is used for the matched disk at interface of IGV/rotor/stator since the 1/7th annulus mesh used for the unsteady simulation is built by copying the single passage mesh.

In Fig. 6, the absolute Mach number and static pressure at 50% span are shown. At the interface of IGV and rotor, and rotor and stator, the flow of the upstream outlet boundary is mixed out to the downstream boundary. The discontinuity from the upstream to the downstream at the mixing plane is obvious. In reality the interaction between two adjacent blade rows in the relative rotation has significant effects on the blade aerodynamic performance such as total pressure loss.

Fig. 7 shows the predicted radial profiles of total pressure ratio, total temperature ratio, absolute flow angle, and adiabatic efficiency at rotor exit. Compared to GE's steady state CFD prediction, all profiles show good agreement. The current results show slightly higher efficiency than GE's steady state CFD results over the 70% span.

## 8 Unsteady Simulation

Unsteady simulation for 1/7th annulus of the multistage compressor was performed over 2 rotor revolutions(2800 physical time steps) with a pseudo time CFL of 1 using the Fourier phase lag BC. The rotor blade passing frequency is used in the phase lag BC for all the blade rows. The number of pseudo time steps within each physical time step is determined by having the residual reduced by at least two orders of magnitude, which usually is achieved within 40 iterations. Physical time step of 1/1400th rotor revolution is used. To reduce CPU time, the flow field for the unsteady simulation is initialized using the mixing plane .

Fig. 8 shows the interface mesh system that enables information exchange in the the fully conservative manner. 1/7th annulus mesh was split into total 174 blocks for the parallel computation. In particular the grid points of 101 in the blade-to-blade was determined to be able to resolve the blade wall boundary layers and wakes.

Fig. 9 illustrates an instant entropy contours, which shows the wake propagation in the blade passage and cross blade rows.

Fig. 10 shows the instantaneous static pressure at 50% span. There are no shocks in the mid-span passage. The instantaneous pressure at the upstream interface of the rotor is measured during the unsteady simulation as shown in Fig. 11. The static pressure fluctuates in the phase locked frequency due to IGV and rotor interaction.

Fig. 12 shows the predicted frequency at 50% span of rotor upstream interface. Blade passing frequency (BPF) is sharply captured.

Fig. 13 compares rotor blade surface pressure distributions at 50%, 98% span respectively. The unsteady results are time averaged for 700 time steps. A significant difference between the steady and the unsteady simulation is shown even though the overall loading is similar, whereas the predicted pressures are almost identical at 50% span. The unsteadiness generated by rotor/stator interaction becomes significant toward rotor tip. The reason may be that the mixing plane method cut off the shock propagation upstream and tip vortex propagation downstream. These two factors ultimately affect the predicted tip loading distribution of the blade.

## 9 Conclusions

This paper simulates the GE 1-1/2 stage compressor using steady state calculation with mixing plane boundary condition and unsteady calculation with sliding boundary conditions. The unsteady sliding boundary conditions are fully conservative without interpolation by always having the grid

point one-to-one connected. The steady state multistage simulation using mixing plane BC agrees well with the results of GE's steady state CFD prediction. The unsteady multistage simulation using sliding BC and phase lag BC predicts almost identical loading distribution to the steady state simulation at the mid-span, but have significant loading distribution difference at tip section. The reason may be that the mixing plane method cut off the shock propagation upstream and tip vortex propagation downstream. These two factors ultimately affect the predicted tip loading distribution of the blade.

**Acknowledgement**

The grants support from AFRL and the industrial partners of GUIde Consortium, 10-AFRL-1024 and 09-GUIDE-1010, are acknowledged. We thank GE for approving publishing the results. .

**References**

[1] J.D. Denton, "The calculation of 3-D viscous flow through multistage turbomachines," *Journal of Turbomachinery*, vol. 114, pp. 18–26, 1992.

[2] W.N. Dawes, "Toward improved throughflow capability: the use of 3-D viscous flow solvers in a multistage environment," *Journal of Turbomachinery*, vol. 114, pp. 8–17, 1992.

[3] U.K. Singh, "A computation and comparison with measurements of transonic flow in an axial compressor stage with shock and boundary-layer interaction," *Journal of Engineering Gas Turbine Power*, vol. 104, pp. 510–515, 1982.

[4] J.W. Barter, P.H. Vitt, and J.P. Chen, "Interaction effects in a transonic turbine stage." ASME paper 2000-GT-0376, Proceedings of ASME Turboexpo 2000, May 8-11 2000, Munich Germany, 2000.

[5] G.A. Gerolymos and C. Hanisch, "Multistage three-dimensional Navier-Stokes computation of off-design operation of a four-stage turbine." Proc Instn Mech Engrs Vol 213 Part A, Third European Conference on Turbomachinery, March 1999, London UK.

[6] G. Fritch and M.B. Giles, "An asymptotic analysis of mixing loss." ASME paper 93-GT-345, 1993.

[7] M. Rai, "Three-dimensional Navier-Stokes simulations of turbine rotor-stator interaction. I - Methodology ," *AIAA Journal of Propulsion and Power*, vol. 5, pp. 305–311, 1989.

[8] M.B. Giles, "Stator/Rotor Interaction in a transonic Turbine," *AIAA Journal of Propulsion and Power*, vol. 6, pp. 621–627, 1990.

[9] L. He, "Three-dimensional unsteady Navier-Stokes analysis of stator-rotor interaction in axial flow turbines," *Proceedings of the Institution of mechanical Engineers, Part A: Journal of Power and Energy*, vol. 214, pp. 13–22, 2000.

[10] A. Ruprecht, C. Bauer, C. Gentner, and G. Lein, "Parallel Computation of Stator-Rotor Interaction in an Axial Turbine." ASME PVP Conference, CFD Symposium, Boston, 1999.

[11] J.P. Chen, and J.W. Barter, " Comparison of time-accurate calculations for the unsteady interaction in turbomachinery stage." AIAA Paper 98-3292, 1998.

[12] J.I. Erods, E. Alzner, and W. McNally, "Numeircal solution of periodic transonic flow through a fan stage," *AIAA Journal*, vol. 15, pp. 1559–68, Nov. 2004.

[13] L. He, and J.D. Denton, "Three-dimensional time marching inviscid and viscous solutions for unsteady flows around vibrating baldes," *Journal of Turbomachinery*, vol. 116, pp. 469–476, 1994.

[14] Zha, G.C., Shen, Y.Q. and Wang, B.Y., "An improved low diffusion E-CUSP upwind scheme ," *Journal of Computer and Fluids*, vol. 48, pp. 214–220, Sep. 2011.

[15] G.C. Zha, Y.Q. Shen, and B.Y. Wang, "Calculation of Transonic Flows Using WENO Method with a Low Diffusion E-CUSP Upwind Scheme." AIAA Paper 2008-0745, 46th AIAA Aerospace Sciences Meeting, Reno, NV, Jan. 2008.

[16] Y.Q. Shen, B.Y. Wang, and G.C. Zha, "Implicit WENO Scheme and High Order Viscous Formulas for Compressible Flows ." AIAA Paper 2007-4431, 2007.

[17] B. Wang, Z. Hu, and G. Zha, "A General Sub-Domain Boundary Mapping Procedure For Structured Grid CFD Parallel Computation," *AIAA Journal of Aerospace Computing, Information, and Communication*, vol. 5, pp. 425–447, 2008.

[18] P.R. Spalart, W.H. Jou, M. Strelets, and S.R. Allmaras, "Comments on the Feasibility of LES for Wings, and on a Hybrid RANS/LES Approach." Advances in DNS/LES, 1st AFOSR Int. Conf. on DNS/LES, Greyden Press, Columbus, H., Aug. 4-8, 1997.

[19] P.R. Spalart, and S.R. Allmaras, "A One-equation Turbulence Model for Aerodynamic Flows." AIAA-92-0439, 1992.

[20] A. Jameson, "Time Dependent Calculations Using Multigrid with Applications to Unsteady Flows Past Airfoils and Wings." AIAA Paper 91-1596, 1991.

[21] H. D Li, and L. He, "Blade Aerodynamic Damping Varaition With Rotor-Stator Gap: A Computational Study Using sinlge-Passage Approach," *Journal of Turbomachinery*, vol. 127, pp. 573–578, Jul. 2005.

[22] H.-S. Im, and G.-C. Zha, " Flutter Prediction of a Transonic Rotor Using a Phase-lagged Boundary Condition." submitted to 50th AIAA Aerospace Sciences Meeting including the New Horizons Forum and Aerospace Exposition, Nashville, Tennessee, Jan 2012, 2012.

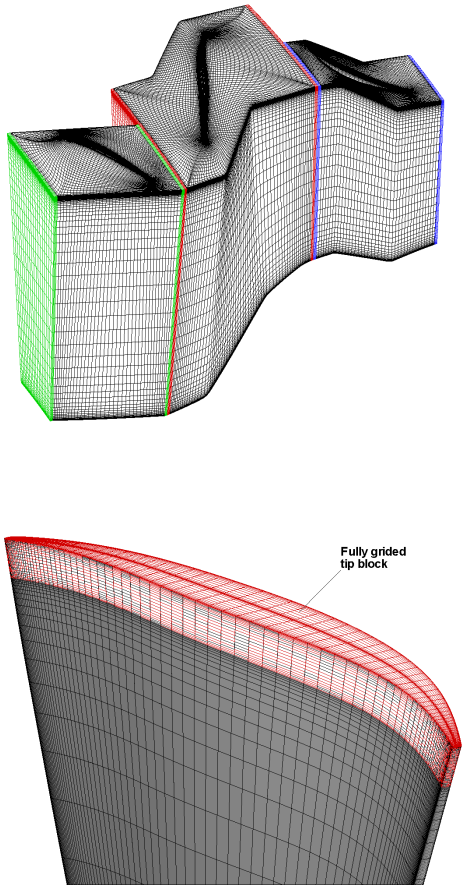


Fig. 5: Single passage mesh for steady mixing plane simulation; IGV=121(around blade) × 51(normal to the blade) × 71(spanwise), Rotor=201× 51× 71, Stator=121× 51×71, tip block = 201×14×21

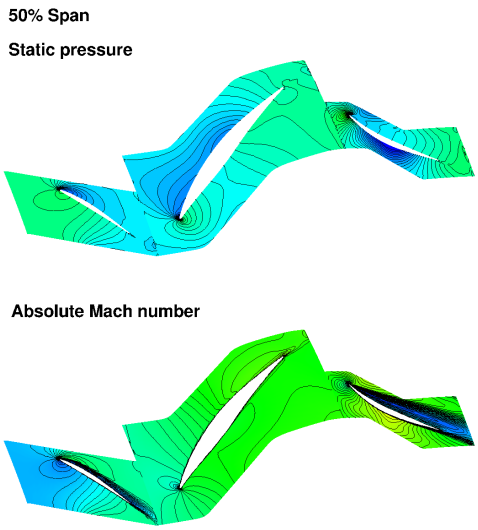


Fig. 6: Mach number and static pressure contour of 50% span predicted by the mixing plane simulation

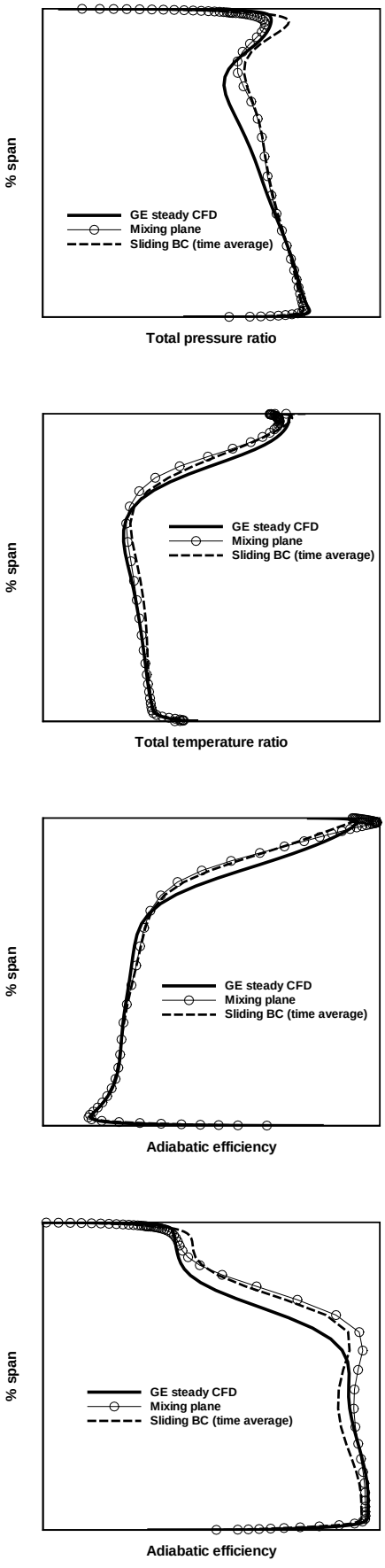


Fig. 7: Predicted pitch-averaged spanwise profiles at rotor exit plane; total pressure, total temperature, absolute flow angle, adiabatic efficiency

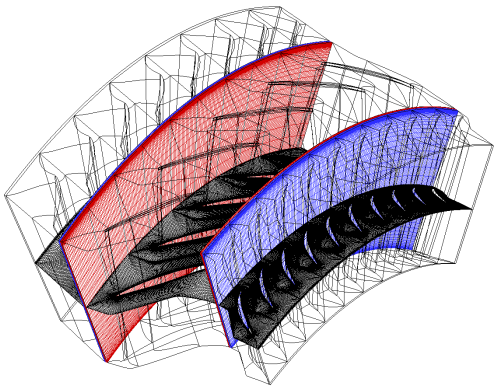

Fig. 8: 1/7th annulus mesh with H-disk blocks at IGV/rotor/stator interface for the unsteady simulation

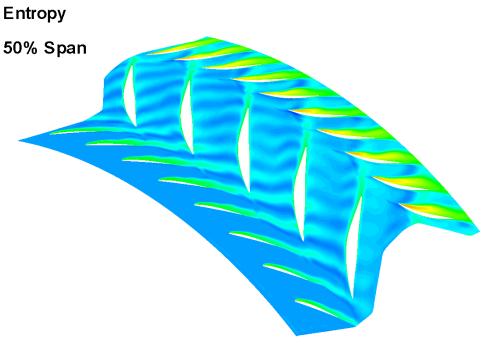


Fig. 9: Entropy at 50% span

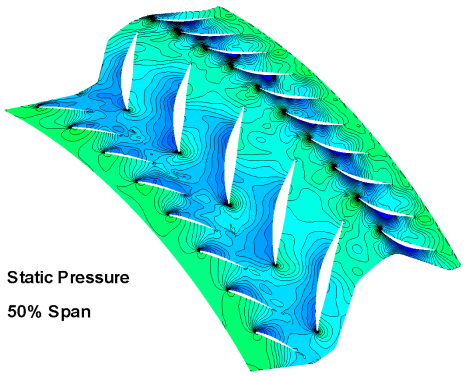


Fig. 10: Static pressure at 50% span

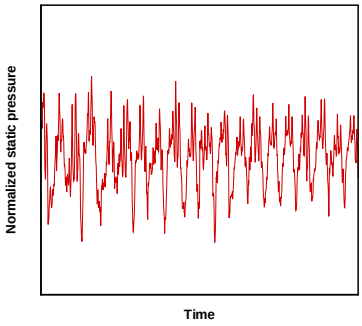


Fig. 11: Static pressure oscillation at the interface of the rotor tip upstream

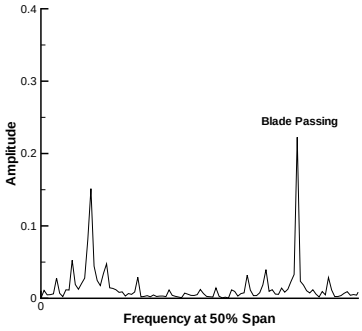


Fig. 12: Predicted blade passing frequency at 50% span of rotor upstream interface

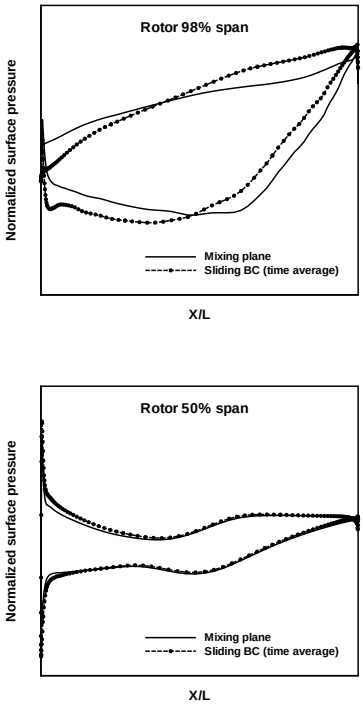


Fig. 13: Distributions of rotor blade surface static pressure at 50% and 98% span